

Enhancing photoassociation rates by nonresonant-light control of shape resonancesRosario González-Férez¹ and Christiane P. Koch²¹*Instituto Carlos I de Física Teórica y Computacional and Departamento de Física Atómica, Molecular y Nuclear, Universidad de Granada, 18071 Granada, Spain*²*Theoretische Physik, Universität Kassel, Heinrich-Plett-Straße 40, 34132 Kassel, Germany*

(Received 9 July 2012; published 26 December 2012)

Photoassociation, assembling molecules from atoms using laser light, is limited by the low density of atom pairs at sufficiently short interatomic separations. Here we show that nonresonant light with intensities of the order of 10^{10} W/cm² modifies the thermal cloud of atoms, enhancing the Boltzmann weight of shape resonances and pushing scattering states below the dissociation limit. This leads to an enhancement of photoassociation rates by several orders of magnitude and opens the way to significantly larger numbers of ground-state molecules in a thermal ensemble than achieved so far.

DOI: [10.1103/PhysRevA.86.063420](https://doi.org/10.1103/PhysRevA.86.063420)

PACS number(s): 34.50.Rk, 32.80.Qk, 33.20.Xx

I. INTRODUCTION

The formation of ultracold molecules ($T \leq 100 \mu\text{K}$) has experienced rapid progress over recent years [1]. At ultralow temperatures, extremely precise control over the molecules' dynamics can be exerted. This allows for transferring molecules into a single quantum state and even for controlling their reactivity [2]. Their rich internal structure makes them sensitive probes in precision measurements of fundamental constants [3]. Possibly strong dipolar interactions facilitate their use in quantum computation and quantum simulation [4].

To produce molecular samples at ultralow temperatures, molecules are typically assembled from ultracold atoms using magnetic-field-controlled Feshbach resonances or laser light. As demonstrated in a series of spectacular experiments, ultracold molecules in their internal ground state are obtained by subsequently applying stimulated Raman adiabatic passage [5–7] or broadband vibrational cooling [8]. However, in all these experiments, the number of ground-state molecules that can be produced has so far been limited to about 10^4 . When the molecules are formed by magnetoassociation, this small number is explained by the very low temperature, of the order of hundreds of nanokelvin, and corresponding high phase-space density, attained, for example, by evaporative cooling. In the case of photoassociation, usually carried out in magneto-optical traps holding up to 10^{10} atoms at temperatures between 1 and $100 \mu\text{K}$ and a phase-space density many orders of magnitude lower, only a small fraction of atom pairs resides at sufficiently short interatomic separations to be photoassociated. The number of ground-state molecules produced directly by photoassociation has thus also been limited to about 10^4 [9]. A significant increase of the photoassociation rate is the problem that we address here.

To this end, we suggest that shape resonances be controlled using nonresonant light to enhance photoassociation rates. Nonresonant light couples to the anisotropic polarizability of an atom pair, shifting the position of shape resonances to lower energies [10] and increasing the resonance's thermal weight in an ultracold trap. Below we demonstrate an enhancement by three orders of magnitude in the photoassociation rate of strontium, a molecule that is currently attracting considerable attention [11–14]. Photoassociation relies only on the

presence of optical transitions, which usually are abundant. Shape resonances are ubiquitous for diatomic molecules. The light-matter coupling via the anisotropic polarizability is of universal character, independent of a particular energy-level structure, frequency of the light, or presence of a permanent dipole moment. Therefore our findings are easily extended to molecules other than Sr₂.

Our approach is related to Feshbach-optimized photoassociation [15], which also employs a scattering resonance to increase the number of atom pairs that are quasitrapped at short interatomic separations. Instead of tuning an existing resonance, one could also use resonances induced by an external field, for example, electric-field-induced resonances for polar molecules [16,17]. However, the electric fields required to achieve a significant enhancement (of about 1.3 MV/cm in the most favorable case) are currently experimentally unfeasible [18]. Unlike Feshbach-optimized photoassociation, shape resonance control does not require the presence of a hyperfine manifold of the atoms. Shape resonances occur naturally for partial waves with $l > 0$ when a scattering state becomes trapped behind the centrifugal barrier. Since shape resonances are quasibound states, they have very favorable free-to-bound overlaps required for efficient photoassociation [see the blue line in Fig. 1 (left)]. In some fortuitous cases such as Rb₂ [20,21] or Cs₂, the energy of a shape resonance almost matches the trap temperature and large photoassociation rates are observed. Typically, however, the lowest energies at which shape resonances occur are far from the trap temperature and their thermal weight is very small. In this case, photoassociation is limited by the atom-pair density $\rho(R)$ at interatomic separations $R \lesssim 200a_0$ [22]; i.e., it addresses mostly s -wave atom pairs for which free-to-bound Franck-Condon factors are very small [see the gray line in Fig. 1 (left)]. This can be changed by applying a strong nonresonant field prior to and during photoassociation.

II. THEORETICAL FRAMEWORK

We assume the nonresonant light, with intensity I , and a photoassociation laser, with intensity I_{PA} , to be linearly polarized along the z axis of the laboratory fixed frame. Then, in the body fixed frame, the interaction of a pair of atoms with

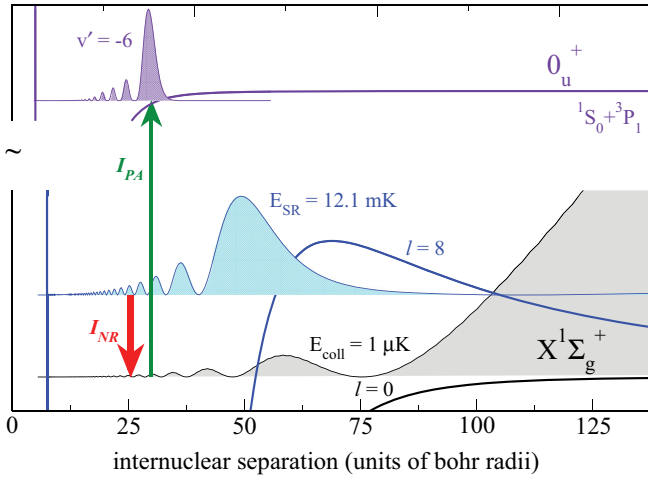


FIG. 1. (Color online) The photoassociation efficiency is determined by the free-bound Franck-Condon overlap between the scattering states and weakly bound excited-state levels (purple line), shown here for photoassociation of $^{88}\text{Sr}_2$ molecules near an intercombination line transition [11,12,19]. For s waves (gray line, scaled by a factor of 10^6 compared to the blue line) the probability density at short internuclear distances is very small, leading to low photoassociation efficiency. A shape resonance (blue line corresponding to a field-free rotational quantum number $l = 8$) is a quasibound state trapped behind the rotational barrier. Typically, its energy E_{SR} is too high for the shape resonance to carry any significant thermal weight in an ultracold cloud. Here we suggest that a strong nonresonant field (red arrow) be employed, which leads to rotational hybridization of the scattering states, effectively moving the position of the shape resonance to lower collision energies E_{coll} and increasing the thermal weight of the shape resonance.

these two fields is described by the Hamiltonian

$$H = \begin{pmatrix} H_g & -\frac{D(R)}{2} \sqrt{\frac{I_{\text{PA}}}{2\epsilon_0 c}} \cos \theta \\ -\frac{D(R)}{2} \sqrt{\frac{I_{\text{PA}}}{2\epsilon_0 c}} \cos \theta & H_e + \Delta_{\text{PA}} \end{pmatrix} \quad (1)$$

with

$$H_j = T + V_j(R) + \frac{\vec{L}^2}{2\mu R^2} - \frac{I}{2\epsilon_0 c} [\Delta\alpha^j(R) \cos^2 \theta + \alpha_{\perp}^j(R)]$$

and $j = g, e$ for the electronic ground and excited states, respectively. Here $\Delta_{\text{PA}} = \hbar(\omega_{\text{PA}} - \omega_{\text{at}})$ denotes the detuning of the photoassociation laser from the atomic resonance and ϵ_0 and c are the electric vacuum permittivity and speed of light. The photoassociation laser interacts with the transition dipole moment $D(R)$ coupling the electronic ground state to an electronically excited state. In addition, $V_g(R)$ and $V_e(R)$ denote the respective potential energy curves and T_R and $\vec{L}^2/2\mu R^2$ are the vibrational and rotational kinetic energies. The nonresonant-light intensity couples to the polarizability anisotropy $\Delta\alpha^j(R) = \alpha_{\parallel}^j(R) - \alpha_{\perp}^j(R)$ ($j = g, e$), where $\alpha_{\parallel(\perp)}^j(R)$ are the parallel and perpendicular molecular polarizability components. The behavior at large internuclear distances is well approximated by Silberstein's formula in terms of atomic polarizabilities [23,24]. We consider ^{88}Sr atoms trapped at a temperature of $1 \mu\text{K}$. The potential energy

curve for the electronic ground state was taken from Ref. [25] and adjusted to yield a scattering length of $a_s = -2a_0$.¹ The potential energy curves for the electronically excited $A^1\Sigma_u^+$, $c^3\Pi_u$, and $a^3\Sigma_u^+$ manifold, spin-orbit coupling functions, and transition dipole matrix elements are found in Ref. [13]. We investigate photoassociation into the lowest level below the $^1S + ^3P$ asymptote that was previously observed ($v' = -6$) [19]. This level is well represented by an adiabatic potential energy curve 0_u^+ neglecting resonant spin-orbit coupling [14]. Its spontaneous emission lifetime was calculated to be $\gamma_{v'=-6} = 7.6 \mu\text{s}$ [14]. The atomic polarizabilities for the ground and excited states are taken from Refs. [26,27]. The Hamiltonian (1) is represented by a mapped Fourier grid for the radial part and a basis set expansion in terms of Legendre polynomials for the angular part, taking advantage of the magnetic quantum number m being conserved. About $N_R \approx 2000$ radial grid points and $l_{\text{max}} = 20$ are required to converge the calculations for $T = 1 \mu\text{K}$ and $I \leq 1.5 \times 10^{10} \text{ W/cm}^2$.

Diagonalizing the Hamiltonian (1) for $I_{\text{PA}} = 0$ yields the bound levels and continuum states of the ground and excited electronic states in the presence of the nonresonant field. For $I \neq 0$, only the magnetic quantum number is conserved. The nonresonant field mixes different partial waves of the same parity and l and l' are no longer good quantum numbers. For the sake of simplicity, we will label the field-dressed states by the field-free quantum numbers l, m, v', l' , and m' , adding a tilde to l, v' , and l' to indicate that they are labels, not quantum numbers. Note that for bound states, the field-dressed levels \tilde{v}' and \tilde{l}' are adiabatically connected to the field-free quantum numbers v' and l' even for very large intensities. The hybridization of the angular motion of the field-dressed wave functions is analyzed in terms of the rotational weights of the field-free partial waves,

$$c_l = \int dE \int R^2 dR \int d\cos\theta \psi_{\tilde{l},0}^s(R, \theta; E_{\text{SR}}) \psi_{l,0}^s(R, \theta; E), \quad (2)$$

where $\psi_{\tilde{l},0}^s(R, \theta; E_{\text{SR}}) = \langle R, \theta | \psi_{\tilde{l}m=0}^s(E_{\text{SR}}) \rangle$ and $\psi_{l,0}^s(R, \theta; E)$ is the field-free scattering wave function for partial wave l . The photoassociation rate coefficient in the presence of the nonresonant field is determined from the excited-state bound levels and ground-state continuum states $|\psi_{\tilde{v}'\tilde{l}m'}^e\rangle$ and $|\psi_{\tilde{l}m}^g(E)\rangle$, respectively, with $|\psi_{\tilde{l}m}^g(E)\rangle$ normalized with respect to energy [28].

For an ensemble of atom pairs with a Maxwell-Boltzmann velocity distribution, employing an isolated photoassociation resonance, the photoassociation rate coefficient is given by [29]

$$K_{\tilde{v}'}(I_{\text{PA}}, \omega_{\text{PA}}, I, T) = \frac{k_B T}{h Q_T} \int_0^\infty \sum_{\tilde{l}=0}^\infty \sum_{\tilde{l}'=0}^\infty e^{-E/k_B T} \times \frac{\gamma_{\tilde{v}'\tilde{l}m'} \gamma_s(I_{\text{PA}}, \tilde{v}', \tilde{l}', m', E, \tilde{l}, m, I)} dE}{(E - \Delta_{\tilde{v}'\tilde{l}m'})^2 + (\gamma/2)^2} \frac{dE}{k_B T}, \quad (3)$$

¹The photoassociation results are not affected when varying the scattering lengths from $a_s = 4.5a_0$ to $a_s = -4.5a_0$.

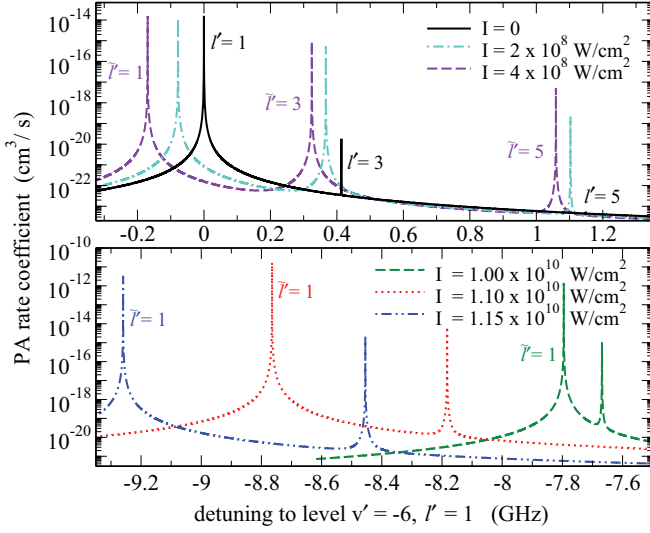


FIG. 2. (Color online) Photoassociation lines (absorption rate coefficient) for photoassociation into $\tilde{v}' = -6$ for weak (top) and strong (bottom) nonresonant fields I . The intensity of the photoassociation laser is set to $I_{\text{PA}} = 1 \text{ W/cm}^2$ and the trap temperature to $T = 1 \mu\text{K}$.

with $\gamma_{\tilde{v}'\tilde{l}'m'}$ the spontaneous decay rate of level $\tilde{v}'\tilde{l}'m'$, approximated by $\gamma_{v'=-6, l'=0, m'=0}$, $\gamma_s \equiv \gamma_s(I_{\text{PA}}, \tilde{v}', \tilde{l}', m', E, \tilde{l}, m, I)$ the stimulated emission rate, and γ the total width, where $\gamma = \gamma_{\tilde{v}'\tilde{l}'m'} + \gamma_s$. Here $Q_T = (2\pi\mu k_B T/h^2)^{3/2}$ denotes the translational partition function and $\Delta_{\tilde{v}'\tilde{l}'m'}$ is the detuning $\Delta_{\tilde{v}'\tilde{l}'m'} = E_{\tilde{v}'\tilde{l}'m'} - \hbar\omega_{\text{PA}}$. Since $^{88}\text{Sr}_2$ is a bosonic molecule with zero nuclear spin, the sum in Eq. (3) runs solely over even partial waves \tilde{l} in the electronic ground state. We consider only $m = m' = 0$ in Eq. (3), for which the effect of the nonresonant field is largest. The actual photoassociation rate will be slightly higher than predicted here due to the neglected contributions from terms with $m \neq 0$ to the sum of Eq. (3). For weak photoassociation intensities, the stimulated emission rate can be approximated by Fermi's golden rule,

$$\begin{aligned} \gamma_s(I_{\text{PA}}, \tilde{v}', \tilde{l}', m', E, \tilde{l}, m, I) \\ \approx \frac{4\pi^2 I_{\text{PA}}}{c} \left| \langle \psi_{\tilde{v}'\tilde{l}'m'}^e | D(R) \cos \theta | \psi_{\tilde{l}m}^g(E) \rangle \right|^2, \end{aligned}$$

i.e., by an integral over R and θ , ensuring the correct selection rules.

III. RESULTS: PHOTOASSOCIATION OF Sr_2

The photoassociation rate $K_{\tilde{v}'}(I_{\text{PA}}, \omega_{\text{PA}}, I, T)$ is shown in Fig. 2 for $\tilde{v}' = -6$ and weak (top) and strong (bottom) nonresonant fields. The black solid line shows the typical rotational progression of a photoassociation spectrum for $I = 0$. The largest peak is observed for $l' = 1$, reflecting the pure s -wave character of the thermal cloud at $1 \mu\text{K}$. A weak nonresonant field (Fig. 2, top) shifts the photoassociation peaks. The largest shift occurs for $\tilde{l}' = 1$. For the optical lattice of Ref. [12] with $I \sim 10^7 \text{ W/cm}^2$, the shift amounts to about 3 MHz. An increase of the peak heights is only observed for $\tilde{l}' = 3$ and 5. It is rationalized in terms of rotational hybridization in the excited-state levels. Generally, bound levels are more strongly affected by the nonresonant field than scattering states. The $\tilde{l}' = 3$ and 5 states thus have

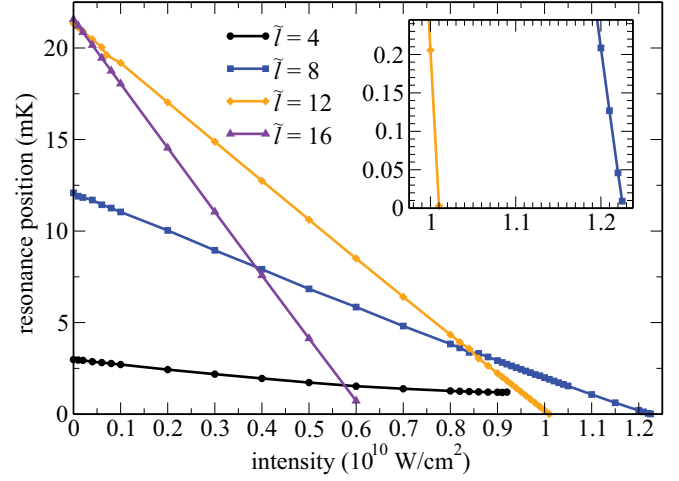


FIG. 3. (Color online) Energy of the $\tilde{l} = 4, 8, 12$, and 16 shape resonances vs nonresonant-field intensity.

some contribution from the $l' = 1$ partial wave that renders photoassociation from s -wave atom pairs into the field-dressed $\tilde{l}' = 3$ and 5 bound state allowed, enhancing the corresponding photoassociation peak. While this increase amounts to several orders of magnitude, the total photoassociation rate for $\tilde{l}' = 3$ and 5 is still smaller than the $l' = 1$ photoassociation rate without a nonresonant field.

At high nonresonant-light intensities (Fig. 2, bottom), the rotational progression observed for $I = 0$ is replaced by the pendular progression. More remarkably, a large increase of the $\tilde{l}' = 1$ peak, amounting to about three orders of magnitude compared to the field-free $l' = 1$ photoassociation rate, is observed in Fig. 2 for nonresonant-field intensities of the order of 10^{10} W/cm^2 . For $T = 1 \mu\text{K}$, the $\tilde{l} = 12$ shape resonance acquires its highest thermal weight close to $I \sim 10^{10} \text{ W/cm}^2$ (see Fig. 3 showing the resonance position as a function of nonresonant-field intensity). The remarkable enhancement of the $\tilde{l}' = 1$ photoassociation rate in Fig. 2 is thus related to the field-dressed $\tilde{l} = 12$ shape resonance. This is further analyzed by inspection of the rotational weights [Eq. (2)] of the field-dressed resonance wave function shown in Fig. 4. The three bottom (two top) panels of Fig. 4 display the components for low (high) l . Note that the coupling mixes only partial waves of the same parity. For $I = 0$, the resonance wave functions are pure $l = 4, 8$, and 12 states, respectively. As the nonresonant field is turned on, a substantial amount of first $l - 2$ and then $l - 4$ is mixed into the field-free states. For large nonresonant-field intensities, the trend of mixing in lower- l components is observed all the way down to $l = 0$ (red diamonds). Thus photoassociation from the field-dressed resonance wave function into $\tilde{l}' = 1$ becomes possible for large I , explaining the large enhancement of photoassociation into an excited-state level with $\tilde{l}' = 1$ observed in the bottom panel of Fig. 2.

While the dependence on the nonresonant intensity in Fig. 4 is smooth for the $\tilde{l} = 4$ resonance, discontinuous behavior is observed for $\tilde{l} = 8$ and 12. Each of the features in the apparently complicated dependence for $\tilde{l} = 8$ and 12 can be rationalized in terms of nonadiabatic behavior of interacting resonances: The first kink in the dependence of

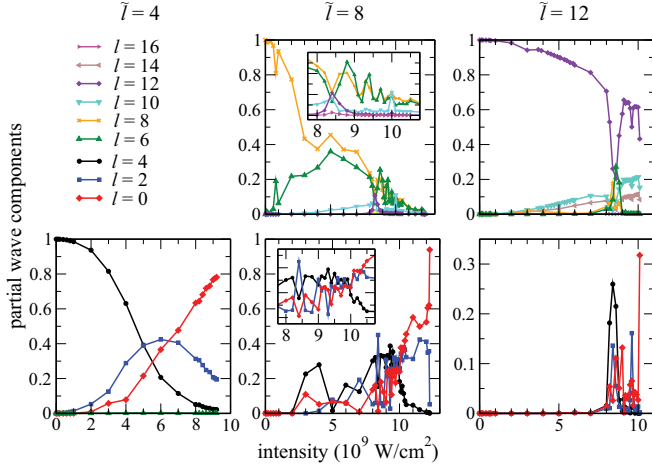


FIG. 4. (Color online) Contribution of different partial waves l to the resonance wave function for the $\tilde{l} = 4, 8,$ and 12 shape resonances as a function of the nonresonant intensity. The low- l contributions are shown in the three bottom panels and the high- l contributions are shown in the two top panels. For high nonresonant-field intensities, all resonance wave functions acquire predominantly s -wave character.

the $\tilde{l} = 8$ resonance is observed at 8×10^8 W/cm². It is due to the interaction with an $\tilde{l} = 6$ shape resonance.² A second discontinuous feature for $\tilde{l} = 8$ is observed around 4×10^9 W/cm². It is caused by the interaction of the $\tilde{l} = 8$ and $\tilde{l} = 6$ resonances close to their crossing (see Fig. 3). The most striking nonadiabatic features occur for both $\tilde{l} = 8$ and 12 resonances between 8×10^9 and 1×10^{10} W/cm². It is due to the nonadiabatic interaction between these two resonances, which cross near 8.5×10^9 W/cm² and with other scattering states, introducing a strong mixing of the resonance wave functions. The nonadiabatic behavior of the shape resonances observed in Fig. 4 underlines the requirement to treat the fully coupled rotational-vibrational dynamics.

The largest increase of the $\tilde{l} = 1$ peak in Fig. 2 is found for $I = 1.10 \times 10^{10}$ W/cm² (red dotted curve). A detailed analysis of the increase as a function of the nonresonant-light intensity is presented in Fig. 5, which shows the height of the $\tilde{l} = 1$ peak normalized with respect to the largest field-free ($l' = 1$) peak. Most importantly, Fig. 5 demonstrates an enhancement of the photoassociation rate between two and three orders of magnitude over a broad range of nonresonant-field intensities. The narrow peaks at $I = 1.01 \times 10^{10}$ and 1.225×10^{10} W/cm² are due to the $\tilde{l} = 12$ and 8 shape resonances (see Fig. 3). These peaks reflect how the shape resonances pass through the energy window that corresponds to the atomic cloud's thermal width. The broad features are attributed to regular scattering states, which are also affected by the nonresonant field. For sufficiently large I , a scattering state is pushed below the dissociation threshold (without symmetry restriction, an even-parity state is followed by an odd-parity

²The $\tilde{l} = 6$ shape resonance can be identified by inspection of the scattering wave functions. However, it is too diffuse for its energy to be determined with sufficient precision and was therefore omitted from Fig. 3.

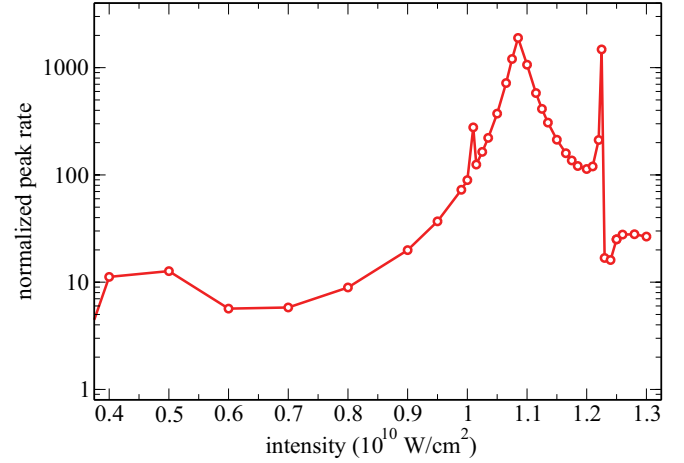


FIG. 5. (Color online) The $\tilde{l} = 1$ peak in the presence of the field normalized with respect to the largest field-free peak (with $l' = 1$) in the rate coefficients for photoassociation into $\tilde{v}' = -6$ ($T = 1$ μ K). Enhancement of the photoassociation rate of about three orders of magnitude is found when the position of a shape resonance comes close to the trap temperature.

state) [17]. Before this happens, the scattering wave function is compressed to short internuclear distances, yielding an increase in the photoassociation rate. This is observed in Fig. 5 for intensities around $I = 1.085 \times 10^{10}$ W/cm². The corresponding state becomes bound at $I \approx 1.22 \times 10^{10}$ W/cm². Also the peak near $I = 5 \times 10^9$ W/cm² is caused by a state being pushed below the dissociation threshold. However, the enhancement is much larger for $I = 1.085 \times 10^{10}$ W/cm² since this state becomes bound in between two shape resonances.

The sharp features of the peak enhancement shown in Fig. 5 clearly reflect the $l = 0$ rotational weight of the $\tilde{l} = 8$ and 12 shape resonances. The small peak at 1.01 W/cm² is connected to the $|c_{l=0}|^2$ weight of the $\tilde{l} = 12$ shape resonance and the sharp rise and drop of the normalized peak rate in Fig. 5 at 1.225 W/cm² reflects the behavior of the $|c_{l=0}|^2$ weight for the $\tilde{l} = 8$ shape resonance before it becomes bound. The $\tilde{l} = 16$ shape resonance, also shown in Fig. 3, suffers almost no hybridization of its angular motion, with $|c_{l=16}|^2$ remaining as high as 0.9 for $I = 6.1 \times 10^9$ W/cm², just before the resonance becomes bound. Therefore, the dipole coupling to $\tilde{v}' = -6, \tilde{l} = 1$ remains rather small and no enhancement due to the $\tilde{l} = 16$ shape resonance is observed in Fig. 5.

In absolute numbers, the maximum peak in Fig. 5 corresponds to a rate of 3×10^{-11} cm³/s, comparable to the photoassociation rates of Cs₂ molecules in weakly bound levels of the $0_g^-(P_{3/2})$ excited state [30]. The important difference from Cs₂ is due to the predominantly $1/R^6$ long-range behavior of the electronically excited state. This allows almost all of the photoassociated molecules to decay into bound ground-state levels and efficient subsequent Raman transfer to low-lying vibrational states.

The bound states of both ground and excited electronic state are characterized by strong alignment in the presence of the nonresonant field [31]. For example, $\langle \cos^2 \theta \rangle \gtrsim 0.94$ for $I \geq 10^{10}$ W/cm². In the presence of the nonresonant field, the photoassociated molecules spontaneously decay into hybridized levels of the electronic ground state. The

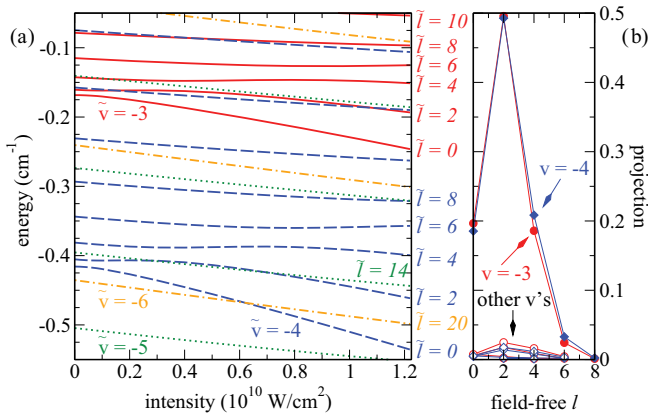


FIG. 6. (Color online) (a) Energy levels and (b) projections of the hybridized $\tilde{v}'' = -3, \tilde{l}'' = 0$ (red) and $\tilde{v}'' = -4, \tilde{l}'' = 0$ (blue) ground-state levels for (a) adiabatic or (b) sudden transfer into their field-free counterparts. For a slow turnoff, nonadiabatic transitions are not expected and all molecules are obtained with $l'' = 0$ (a), while for a sudden turnoff, about 20% of the molecules have $l'' = 0$ and about 50% have $l'' = 2$.

branching ratios are calculated from the transition dipole moments [14] of the field-dressed rovibrational states. For $I = 1.1 \times 10^{10}$ W/cm², $\tilde{v}' = -6, \tilde{l}' = 1$ shows a branching ratio of 31% to $\tilde{v}'' = -3, \tilde{l}'' = 0$ and 43% to $\tilde{v}'' = -4, \tilde{l}'' = 0$ compared to field-free branching ratios of 51% and 41% for $v'' = -3, l'' = 0$ and $v'' = -3, l'' = 2$, respectively.³ Once molecules in the electronic ground state are produced, the nonresonant field has to be turned off. If this is done adiabatically, the hybridized ground-state levels $\tilde{v}'' = -3, \tilde{l}'' = 0$ and $\tilde{v}'' = -4, \tilde{l}'' = 0$ are directly connected with $v'' = -3, l'' = 0$ and $v'' = -4, l'' = 0$. A slow turnoff of the nonresonant field transfers these hybridized levels to their field-free counterparts unless avoided level crossings occur. For $\tilde{v}'' = -3, \tilde{l}'' = 0$ and $\tilde{v}'' = -4, \tilde{l}'' = 0$, crossings may be found only for very highly excited rotational states from lower vibrational bands $\tilde{l}'' \geq 20$ for which the nonadiabatic couplings with $l'' = 0$ are small [see Fig. 6(a)]. A slow turnoff of the nonresonant field thus produces ground-state molecules with $v'' = -3$ or -4 and $l'' = 0$. If the molecules after spontaneous decay are subject to loss processes in the trap, it may not be possible to turn off the field adiabatically. A sudden turnoff projects the hybridized ground-state levels onto a superposition of $m' = 0$ field-free rotational levels of the same vibrational band with about 50% $l'' = 2$, 20% $l'' = 0$, and 20% $l'' = 4$ components for both $v'' = -3$ and -4 [see Fig. 6(b)]. Thus a large part of the molecules is transferred to ground vibrational levels with $l'' = 0$ for both slowly or suddenly turning off the field. The weakly bound ground-state levels show large two-photon transition matrix elements for efficient Raman transfer to low-lying rovibrational levels of the electronic ground state [14]. Almost all of the molecules produced by photoassociation can thus be transferred to the rovibrational ground state, in contrast to all previous photoassociation schemes realized experimentally to date.

³The field-free branching ratios differ slightly from those published in Ref. [14] due to the adiabatic approximation for the 0_u^+ state employed here.

IV. CONCLUSION

We have shown that the photoassociation rate of Sr₂ molecules is enhanced by three orders of magnitude by applying an additional nonresonant field. This enhancement is due to shape resonances and scattering states becoming bound, causing a larger number of atom pairs to be quasitrapped at sufficiently short interatomic separations to be photoassociated. Since the photoassociation rate is limited by the low pair density at or near the Condon radius [22,32], applying strong nonresonant light during photoassociation overcomes the main obstacle toward forming larger numbers of molecules. The enhancement of the photoassociation rate is accompanied by strong hybridization of the angular motion, which we have fully accounted for in a rigorous treatment of the coupled rovibrational motion.

Prior to photoassociation, the nonresonant field needs to be turned on slowly such that the position of shape resonances and scattering states is shifted adiabatically to lower energies. Then the photoassociation laser addresses a thermal cloud that is modified by the nonresonant light, producing molecules in an electronically excited state. As a specific feature of photoassociation near an intercombination line, the majority of photoassociated molecules decays spontaneously into bound ground-state levels rather than redissociate [14,19]. In the presence of the nonresonant field, the spontaneous emission involves hybridized levels. To obtain field-free ground-state molecules, the nonresonant field needs to be turned off. Ideally, this is done adiabatically, yielding rotationless molecules in two ground-state vibrational levels. Alternatively, a sudden turnoff leads to a superposition of ground-state molecules with the three lowest rotational quantum numbers 0, 2, and 4 occupied.

The required nonresonant-field intensities of the order of 10^{10} W/cm² can be achieved by employing intracavity beams. Assuming a spot size of the order of 10 μ m, intracavity powers of up to 10^4 W are needed. Such powers can realistically be produced, for example, by injecting 100 W from a single-mode telecommunications wavelength fiber laser into a cavity with a power buildup factor of 100.

Enhanced photoassociation rates are a crucial prerequisite to increase the number of ground-state molecules that can be produced optically. For molecules other than Sr₂, our scheme works best for heavy atoms with large polarizabilities and large scattering lengths. Promising candidates include, besides other even-isotope alkaline-earth-metal dimers or Yb₂, heteronuclear molecules comprised of one alkali-metal atom and one alkaline-earth-metal-like atom such as RbSr or RbYb [33]. For these species, where Feshbach association is either not available or likely not feasible [34], nonresonant-field control of shape resonances paves the way for an efficient all-optical production of ground-state molecules.

ACKNOWLEDGMENTS

We would like to thank Anne Crubelier, Michael Drewsen, Ronnie Kosloff, Eliane Luc-Koenig, and Robert Moszyński for fruitful discussions. Financial support by the Spanish Project No. FIS2011-24540 (MICINN) as well as the Grants No. FQM-2445 and No. FQM-4643 (Junta de Andalucía) is gratefully acknowledged. R.G.-F. belongs to the Andalusian research group FQM-207.

- [1] *Cold Molecules: Theory, Experiment, Applications*, edited by R. V. Krems, W. C. Stwalley, and B. Friedrich (CRC, Boca Raton, FL, 2009).
- [2] S. Ospelkaus, K.-K. Ni, D. Wang, M. H. G. de Miranda, B. Neyenhuis, G. Quémener, P. S. Julienne, J. L. Bohn, D. S. Jin, and J. Ye, *Science* **327**, 853 (2010).
- [3] T. Zelevinsky, S. Kotochigova, and J. Ye, *Phys. Rev. Lett.* **100**, 043201 (2008).
- [4] A. Micheli, G. K. Brennen, and P. Zoller, *Nat. Phys.* **2**, 341 (2006).
- [5] F. Lang, K. Winkler, C. Strauss, R. Grimm, and J. Hecker Denschlag, *Phys. Rev. Lett.* **101**, 133005 (2008).
- [6] K.-K. Ni, S. Ospelkaus, M. H. G. de Miranda, A. Pe'er, B. Neyenhuis, J. J. Zirbel, S. Kotochigova, P. S. Julienne, D. S. Jin, and J. Ye, *Science* **322**, 231 (2008).
- [7] J. G. Danzl, E. Haller, M. Gustavsson, M. J. Mark, R. Hart, N. Bouloufa, O. Dulieu, H. Ritsch, and H.-C. Nägerl, *Science* **321**, 1062 (2008).
- [8] M. Viteau, A. Chotia, M. Allegrini, N. Bouloufa, O. Dulieu, D. Comparat, and P. Pillet, *Science* **321**, 232 (2008).
- [9] J. Deiglmayr, A. Grochola, M. Repp, K. Mörtlbauer, C. Glück, J. Lange, O. Dulieu, R. Wester, and M. Weidemüller, *Phys. Rev. Lett.* **101**, 133004 (2008).
- [10] R. Aĝanoĝlu, M. Lemeshko, B. Friedrich, R. González-Férez, and C. P. Koch, arXiv:1105.0761.
- [11] S. Stellmer, B. Pasquiou, R. Grimm, and F. Schreck, *Phys. Rev. Lett.* **109**, 115302 (2012).
- [12] G. Reinaudi, C. B. Osborn, M. McDonald, S. Kotochigova, and T. Zelevinsky, *Phys. Rev. Lett.* **109**, 115303 (2012).
- [13] W. Skomorowski, F. Pawłowski, C. P. Koch, and R. Moszynski, *J. Chem. Phys.* **136**, 194306 (2012).
- [14] W. Skomorowski, R. Moszynski, and C. P. Koch, *Phys. Rev. A* **85**, 043414 (2012).
- [15] P. Pellegrini, M. Gacesa, and R. Côté, *Phys. Rev. Lett.* **101**, 053201 (2008).
- [16] R. V. Krems, *Phys. Rev. Lett.* **96**, 123202 (2006).
- [17] R. González-Férez and P. Schmelcher, *New J. Phys.* **11**, 055013 (2009).
- [18] D. Chakraborty, J. Hazra, and B. Deb, *J. Phys. B* **44**, 095201 (2011).
- [19] T. Zelevinsky, M. M. Boyd, A. D. Ludlow, T. Ido, J. Ye, R. Ciuryło, P. Naidon, and P. S. Julienne, *Phys. Rev. Lett.* **96**, 203201 (2006).
- [20] H. M. J. M. Boesten, C. C. Tsai, B. J. Verhaar, and D. J. Heinzen, *Phys. Rev. Lett.* **77**, 5194 (1996).
- [21] H. M. J. M. Boesten, C. C. Tsai, J. R. Gardner, D. J. Heinzen, and B. J. Verhaar, *Phys. Rev. A* **55**, 636 (1997).
- [22] C. P. Koch, R. Kosloff, E. Luc-Koenig, F. Masnou-Seeuws, and A. Crubellier, *J. Phys. B* **39**, S1017 (2006).
- [23] T. G. Heijmen, R. Moszyński, P. E. Wormer, and A. van der Avoird, *Mol. Phys.* **89**, 81 (1996).
- [24] L. Jensen, P.-O. Åstrand, A. Osted, J. Kongsted, and K. V. Mikkelsen, *J. Chem. Phys.* **116**, 4001 (2002).
- [25] A. Stein, H. Knöckel, and E. Tiemann, *Phys. Rev. A* **78**, 042508 (2008).
- [26] *CRC Handbook of Chemistry and Physics*, 91st ed., edited by D. R. Lide (Taylor and Francis, London, 2009).
- [27] S. G. Porsev, A. D. Ludlow, M. M. Boyd, and J. Ye, *Phys. Rev. A* **78**, 032508 (2008).
- [28] R. González-Férez, M. Weidemüller, and P. Schmelcher, *Phys. Rev. A* **76**, 023402 (2007).
- [29] R. Napolitano, J. Weiner, C. J. Williams, and P. S. Julienne, *Phys. Rev. Lett.* **73**, 1352 (1994).
- [30] A. Fioretti, D. Comparat, A. Crubellier, O. Dulieu, F. Masnou-Seeuws, and P. Pillet, *Phys. Rev. Lett.* **80**, 4402 (1998).
- [31] B. Friedrich and D. Herschbach, *Phys. Rev. Lett.* **74**, 4623 (1995).
- [32] C. P. Koch, R. Kosloff, and F. Masnou-Seeuws, *Phys. Rev. A* **73**, 043409 (2006).
- [33] F. Münchow, C. Bruni, M. Madalinski, and A. Görlitz, *PhysChemChemPhys* **13**, 18734 (2011).
- [34] D. A. Brue, and J. M. Hutson, *Phys. Rev. Lett.* **108**, 043201 (2012).